FABRICATION OF SUPERHYDROPHOBIC STRUCTURES VIA AEROSOL JET PRINTING

Jace Rozsa[1], Ke Zhong[1], Dinesh K. Patel[1], Lining Yao[2] Mohammad F. Islam[1] and Gary K. Fedder[1]*
[1]Carnegie Mellon University, Pittsburgh, Pennsylvania, USA
[2]University of California, Berkeley, USA

ABSTRACT

A scalable, one-step method for creating superhydrophobic surfaces is presented. The central mechanism is solvent evaporation during aerosol transport in an aerosol jet printer, leading to gelated polymer micro-spheres. The material printed in this study is disulfide-polydimethylsiloxane, though the method is generalizable to other materials. Aerosol behavior using two solvents spanning a two decade range of vapor pressures is modeled and supported with experimental evidence. Various demonstrations involving microfluidic manipulation are presented.

KEYWORDS

Superhydrophobic, aerosol jet printing, disulfide-polydimethylsiloxane, microfluidics.

INTRODUCTION

Superhydrophobic surfaces perform many functions in nature [1-3] as well as in technology [4-7]. There are two sources of superhydrophobicity: the intrinsic chemical structure of the material or its morphology [8,9]. A material is considered superhydrophobic if it exhibits a contact angle of greater than 150° and a low sliding angle of less than 10° [10,11].

Many methods for producing superhydrophobic materials have been studied, they include hydrothermal synthesis [12], vapor deposition [13], and lithography [14], among others [15,16]. These techniques are often limited in their scale by complex process steps or time-consuming operation. Simpler methods such as spray coating [17], dip coating [18], and electrospinning [19] stand as an alternative, though these methods are often imprecise and lack controllability. They also oftentimes require materials that are already highly hydrophobic through their intrinsic material properties. Additive manufacturing techniques have been found to be effective in creating superhydrophobic structures [7, 20, 21], though these methods also suffer from the same setbacks of poor scalability and the necessity for post processing.

We present a method for creating superhydrophobic structures by aerosolization of polymer ink followed by high spatial resolution deposition through aerosol jet (AJ) printing. Using this technique, spherical microgel polymer particles are deposited directly onto a surface, creating a micro-scale surface roughness that causes the surface to become superhydrophobic (figure 1).

The polymer used in the present study is disulfide-polydimethylsiloxane (DS-PDMS), a weakly hydrophobic polymer, which reflows at temperatures above 90 °C and solidifies again when cooled below 90 °C. The presented method requires no pre- or post-processing, making it highly versatile. We can also create spatially complex structures with feature dimensions on the order of tens of μm by leveraging the capabilities of AJ printing.

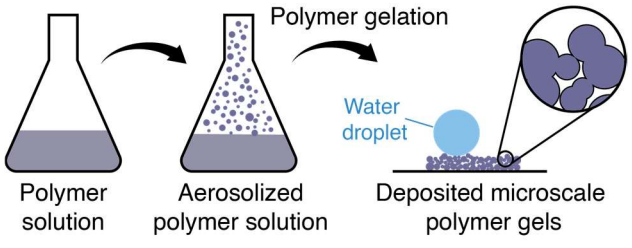

Figure 1: Process of ink aerosolization and resulting superhydrophobic structure after gelled aerosol droplets have been deposited.

METHODS

Aerosol Jet Printing of DS-PDMS

Aerosol jet 3D printing is a microfabrication technology that generates and deposits aerosol droplets with high spatial precision, producing three-dimensional structures with feature sizes in the tens of microns [22]. Illustrated in Figure 2A, AJ printing begins with aerosolization of an ink using ultrasonication. The aerosolized droplets are transported by an inert carrier gas (nitrogen) through a tube to the deposition head. In the deposition head, a sheath gas (nitrogen) is introduced to focus the incoming stream of droplets (figure 2B). Upon leaving the nozzle, the droplets form a tightly focused, collimated beam where they are deposited on the print surface [25].

The material used to create superhydrophobic surfaces was DS-PDMS synthesized by incorporating disulfide (DS) bonds into PDMS polymer chains. The three reactants used for the synthesis are aminopropyl terminated polydimethylsiloxane (PDMS-NH_2), isophorone diisocyanate (IPDI), and bis(2-hydroxyethyl) disulfide (HEDS). DS-PDMS gels at a low concentration of 62 vol%. To verify this, DS-PDMS was dissolved in tetrahydrofuran (THF) to form a 25 vol% solution, which was exposed to air to allow the THF to evaporate. The onset of gelation was identified by the absence of observable flow when the vial was inverted. The gelation concentration, calculated based on the volume change pre- and post-gelation, was found to be 62±2 vol%.

Droplet Evaporation Model

If polymer gelation occurs before the aerosol droplets are deposited on the printing substrate, the droplets will collide and adhere in gel form on the substrate. These droplets have insufficient solvent to reflow upon impact and thus retain their spherical form.

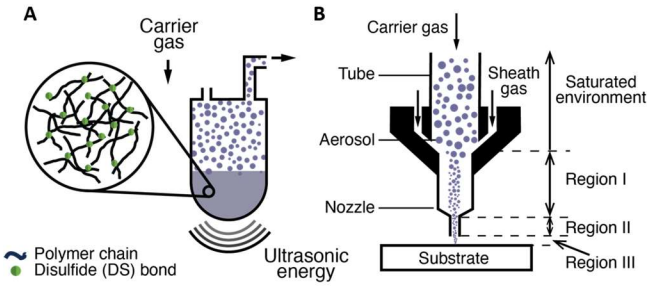

Figure 2: Aerosol jet printing system: A) aerosol generation of DS-PDMS by ultrasound. Magnified portion of image shows PDMS polymer chains with disulfide bonds. B) Cross sectional view of AJ nozzle, in which carrier gas is focused by the introduction of a sheath gas, and then further focused through constriction by the nozzle. Diagram denotes three regions of distinct geometry in which the solvent in an aerosol droplet will evaporate.

978-1-940470-05-4/HH2024/$25©2024TRF
DOI 10.31438/TRF.HH2024.24

The result is the formation of microstructures that contribute to the superhydrophobicity of the printed structure (figure 1). Conversely, if polymer gelation has not occurred before reaching the print surface, the aerosol droplet remains in a liquid state and multiple droplets coalesce to form a relatively smooth surface before the polymer gels. In this latter case, relatively few microstructures are present on the surface to contribute to the hydrophobicity of the structure.

We used a droplet evaporation model to better understand the aerosol evaporation dynamics occurring in the AJ printer and to predict the printed surface structure. For the following calculations, the aerosol droplets are assumed to be spherical, and the effect of solute on the evaporation process is neglected. The solvent mass loss per unit time is calculated using the Stefan-Fuchs model [23,24]:

$$\dot{m}_a = -4\pi R_a D_v \rho_{total} \ln(1 + B_M) \quad (1)$$

where R_a is the radius of an aerosol droplet, D_v is the diffusion coefficient of the vapor phase, ρ_{total} is the total mass density of the vapor and gas phases, and B_M is the Spalding mass transfer number. The total mass density of the gas-vapor mixture is:

$$\rho_{total} = \rho_v + \rho_g = \frac{M_v P_v}{RT} + \frac{M_g P_g}{RT} \quad (2)$$

where M_v and M_g are the molecular weights of the vapor (solvent) and the gas, respectively. P_v and P_g are partial pressures of the vapor (solvent) and the gas, respectively. The Spalding mass transfer number is:

$$B_M = \frac{\rho_{v,\,s} - \rho_{v,\infty}}{\rho_{g,s}} \quad (3)$$

where $\rho_{v,\,s}$ and $\rho_{v,\infty}$ are densities of vapor in the vicinity of the aerosol droplet and in free space, respectively, and $\rho_{g,s}$ is the density of ambient gas. Figure 2B shows a detailed schematic of the deposition head of the AJ printer, including the areas where the aerosol begins to undergo solvent evaporation. Prior to the introduction of sheath gas, a saturated environment is assumed [25], which results in negligible solvent evaporation and a largely stable droplet size. Once the sheath gas is introduced, the vapor density away from the aerosol droplet is expected to be $\rho_{v,\infty} = \frac{1}{3}\rho_{v,\,s}$ because the gas flow rate ratio between the saturated carrier gas and the sheath gas is set to 1:2. The solvent evaporation occurs in three separate regions, each of which feature distinct characteristics that will affect the values for equations (1)-(3).

- Region I: the nozzle has a diameter of approximately 650 µm and a length of around 20.5 mm (inclusive of the connector and the thicker part of the nozzle). The gas is nitrogen for equations (2) and (3).
- Region II: this section of the nozzle is much thinner with a diameter of 150 µm and a length of around 4.5 mm. The gas is also nitrogen.
- Region III: the aerosol is ejected from the nozzle. The distance between the nozzle and the substrate is set to 2 mm and the gas is now ambient air rather than nitrogen.

The different diameters resulted in varying flight speeds of the aerosol droplet in the two sections, given the constant gas flow. The total flight time in Region III before the droplets reach the substrate was found to be: $t = 5.5 \times 10^{-6}$ s. As the evaporation rate is dependent on the droplet radius, the evaporation rate and resulting polymer concentration within the droplet was iteratively calculated using a relatively small timestep ($dt = 10^{-7}$ s).

The plots of figures 4A and 4B show the calculations of polymer concentration in the aerosol droplets as a function of time for two solvents: THF and dimethylformamide (DMF). The plots terminate when the droplets reach the gelation concentration of 62 vol%, at which point we assume that the droplets' concentration remains constant. This is illustrated by the horizontal dashed line in the figures. The vertical line contained in each plot represents the droplets' flight time from the point that solvent evaporation begins to the moment it reaches the substrate. The various curves show the calculation for different initial radii of the aerosol droplets. THF has a vapor pressure of $P_{v,THF} = 127.5$ mmHg as compared to $P_{v,DMF} = 2.8$ mmHg for DMF. From the model, this increased volatility leads to gelling of droplets with initial radii up to 7 µm for THF, while for DMF, the maximum initial radii of droplets to gel is around 1 µm. The aerosol droplets generated at the ultrasonic source are assumed to vary in size from 0.5 to 2.5 µm in radius [25]. This suggests that the aerosol droplets with THF will be mostly void of solvent by the time they reach the printing substrate. For droplets generated with DMF, on the other hand, only those with initial radii from 0.5 to 1 µm are expected to undergo gelation. The majority of droplets retain solvent content, promoting coalescence. We can therefore predict that gelled droplets for structures printed with DMF solvent will be smaller than those printed with THF.

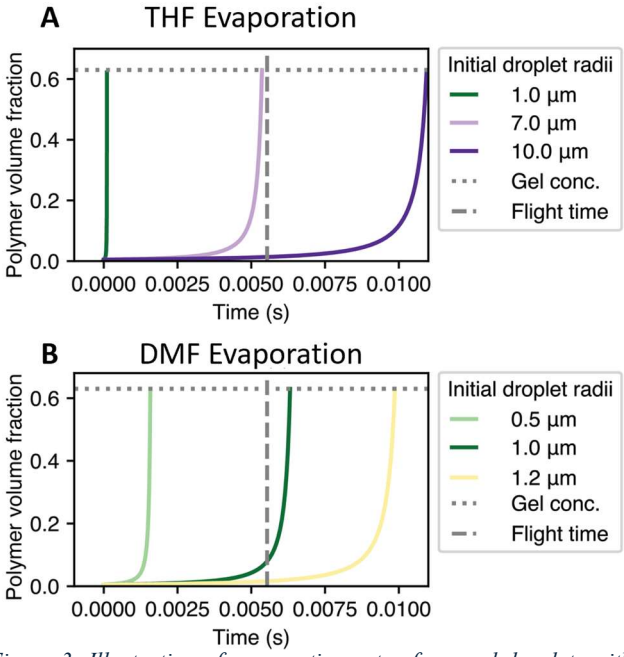

Figure 3: Illustration of evaporation rate of aerosol droplets with A) THF and B) DMF as solvents. Horizontal dotted line denotes point at which the aerosol becomes gelled, vertical dotted line is the travel time for an aerosol droplet during which the droplet is losing solvent through evaporation.

RESULTS

Model Verification

We validate our prediction with the morphology and contact angle measurement of the printed surfaces with DS-PDMS aerosol jetting using the two different solvents in figure 3A and B. For each of the experiments, the printed structure was a 5 mm x 5 mm continuous patch, composed of two layers, with each layer formed by repeatedly printing parallel lines adjacent to each other with an 80 µm pitch. The orientation of the lines of the second layer was orthogonal to that of the first. The print substrate was heated to 40 °C to speed evaporation of any remaining solvent upon droplet impact.

Figure 4A shows an SEM image of a printed sample utilizing THF as the solvent. The image reveals a surface morphology

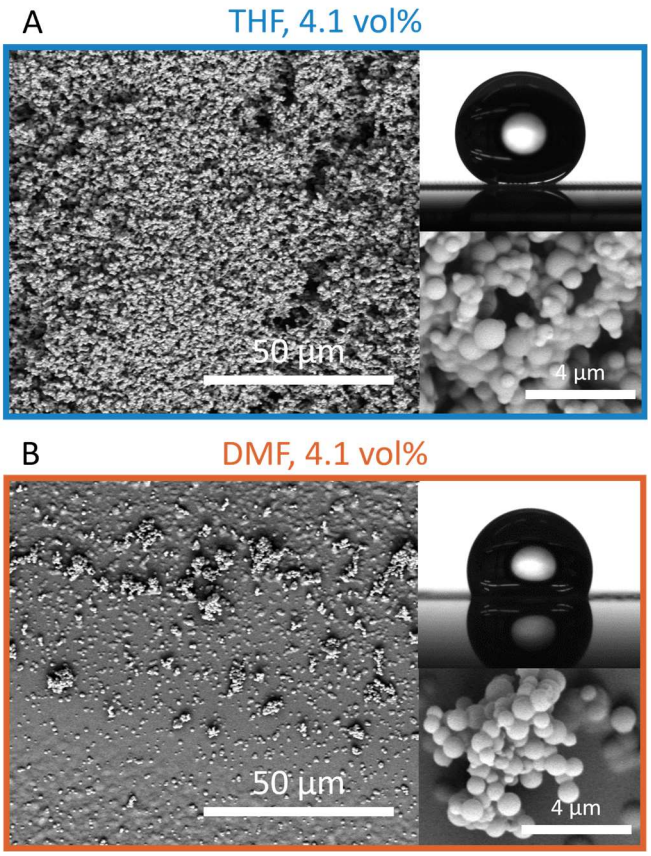

Figure 4 (3): SEM images of structure printed with A) THF and B) DMF solvents. Both inks were mixed with a 4.1% polymer to solvent ratio.

characterized by microscale spherical particles, nearly fully intact with very little coalescence between adjacent spheres. This suggests that all droplets were fully gelled upon impact with the print surface. To compare, figure 4B shows an SEM image taken from a structure that was printed using DMF as the solvent. This sample shows a relatively smooth substrate with only small intact spheres remaining on the surface. These intact spheres are few in number when compared with those of figure 4A. The smoothness of the printed substrate in figure 4B confirms that most droplets still contain a significant amount of solvent upon incidence with the print surface, as these droplets readily congeal with the material already present. The relatively small size of the droplets that did not congeal concurs with the calculations illustrated in figure 3B in which we expect that only droplets with an initial radius of less than 1 µm will have gelled by the time they reach the substrate.

It is also worth noting that the image in figure 4B shows a line of relatively smooth material, with the spheres gathered on each side of this smooth region. This is due to the overspray that results from AJ printing [25]. Collimated flow lines leaving the nozzle begin to diverge upon approaching the print surface. The largest droplets will continue their linear trajectory and impact the print surface, but the smaller droplets do not have the momentum to overcome the force from the diverging flow lines and are carried away from their original trajectory, eventually impacting the print surface at a location shifted laterally from the nozzle. These overspray droplets are gelled by the time they reach the print surface and therefore cannot fully congeal with the already present structure, which by this time has also begun to solidify due to the heated print surface.

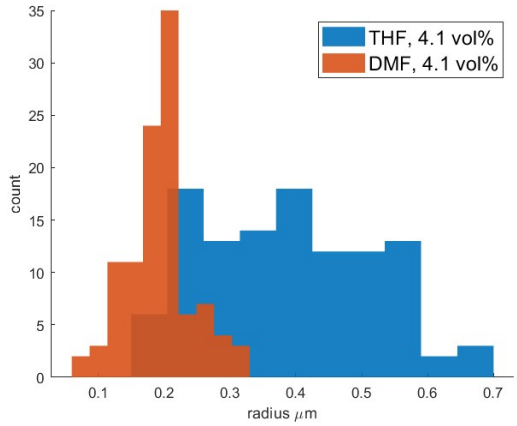

Figure 5: Size distribution of spheres found in SEM images. Images were analyzed using ImageJ

This leads to spheres shown in the magnified portion of figure 4B in which some are partially congealed while others remain fully intact on the surface.

To quantify the hydrophobicity of these structures, we used a goniometer (Rame-Hart, Model 100-00-115) to measure the contact angle formed with a 5 µL drop placed on the surface of the printed structure. Each measurement was taken three times. The THF structure exhibited superhydrophobicity, with an average contact angle of 160°. The DMF structure showed an average hydrophobicity of 113°, which is still higher than the intrinsic hydrophobicity of DS-PDMS (99° contact angle for drop-cast sample).

To further confirm our theory, we measured the sizes of the spheres from the samples shown in figure 4A and B. This was done by analyzing the SEM images with ImageJ. The resulting size distribution is shown in figure 5. For the THF print, 0.39 µm is the average sphere radius while for the DMF print it is 0.19 µm. This nearly 3x difference in radius is explained by the presented model.

Applications

AJ printing can produce features as small as 25 µm in size. This is useful for creating structures for various microfluidic applications, from drug screening to in-droplet chemical synthesis. One potential use case for this technique is droplet mixing for micro reaction. Figure 6A shows an arc-shaped channel in which a droplet is dispensed on each extreme of the structure. The wafer was tilted at approximately 45°, and the two droplets follow the channel until they meet at the reservoir and are mixed, facilitating controlled

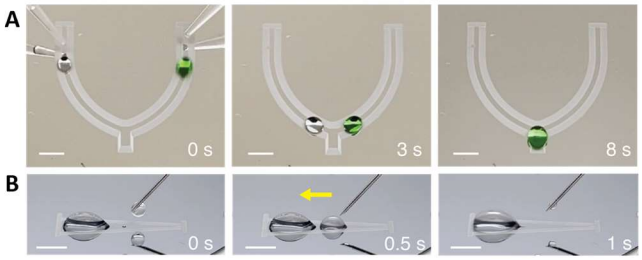

Figure 6: Demonstration of applications for this technology A) microdroplet mixing. Droplets are placed at each end of the structure and when the substrate is tilted the printed DS-PDMS guides the droplets into the mixing reservoir. B) Demonstration of the ability of a tapered channel to cause a droplet to move without the need for tilting.

microscale-volume reactions. We can initiate droplet motion without the need to tilt the substrate by printing tapered channels in which a dispensed water droplet will tend to move toward the wider end of a channel. This effect occurs because the energy state at the larger end of the channel is lower than that at the smaller end for a given droplet size. Figure 6B shows how this phenomenon can be used to produce movement in the droplet without any wafer tilting or applied agitation force.

CONCLUSION

We have demonstrated a new technique for creating superhydrophobic structures that exhibit superhydrophobicity beyond the intrinsic hydrophobicity of the underlying material. The primary mechanism for this result is the solvent evaporation of aerosol droplets before reaching the print surface. This mechanism has been studied using an analytical model and experimentally verified. We also varied the inputs to the process and the experimental results agree with predictions from the analytical model. This technique has been demonstrated using DS-PDMS but the gelation in aerosol is a general behavior that can extend to many other polymers in principle. Demonstration of the potential uses for this phenomenon with a variety of application examples motivates use of this method with AJP for achieving fine patterning of superhydrophobic features.

ACKNOWLEDGEMENTS

K.Z. and J.R. contributed equally to this work. This work is supported by Manufacturing Futures Institute (MFI) 2023 seed funding program at Carnegie Mellon University through a grant from the Richard King Mellon Foundation. The authors acknowledge support from the National Science Foundation Career Grant IIS-2047912 (LY).

REFERENCES

[1] T. Darmanin, F. Guittard, “Superhydrophobic and superoleophobic properties in nature", *Materials Today* 2015, 18, 273

[2] Z. Guo, W. Liu, “Biomimic from the superhydrophobic plant leaves in nature: Binary structure and unitary structure”, *Plant Science* **2007**, *172*, 1103

[3] S. Ge-Zhang, T. Cai, H. Yang, Y. Ding, M. Song, “Biology and nature: Bionic superhydrophobic surface and principle”, *Front. Bioeng. Biotechnol.* **2022**, *10*, 1033514

[4] Y. Si, Z. Dong, L. Jiang, “Bioinspired designs of superhydrophobic and superhydrophilic materials”, *ACS Cent. Sci.* **2018**, *4*, 1102

[5] H. Pakzad, M. Liravi, A. Moosavi, A. Nouri-Borujerdi, H. Najafkhani, “Fabrication of durable superhydrophobic surfaces using PDMS and beeswax for drag reduction of internal turbulent flow”, *Applied Surface Science* **2020**, *513*, 145754

[6] S. Xu, Q. Wang, N. Wang, “Chemical fabrication strategies for achieving bioinspired superhydrophobic surfaces with micro and nanostructures: a review”, *Advanced Engineering Materials* **2021**, *23*, 2001083.

[7] Y. Yang, X. Li, X. Zheng, Z. Chen, Q. Zhou, Y. Chen, “3D-Printed Biomimetic Super-Hydrophobic Structure for Microdroplet Manipulation and Oil/Water Separation”, *Advanced Materials* **2018**, *30*, 1704912.

[8] E. Celia, T. Darmanin, E. T. de Givenchy, S. Amigoni, F. Guittard, “Recent advances in designing superhydrophobic surfaces”, *Journal of Colloid and Interface Science* **2013**, *402*, 1.

[9] T. Kong, G. Luo, Y. Zhao, Z. Liu, “Bioinspired Superwettability Micro/Nanoarchitectures: Fabrications and Applications”, *Adv Funct Materials* **2019**, *29*, 1808012.

[10] W. Zhang, D. Wang, Z. Sun, J. Song, X. Deng, “Robust superhydrophobicity: mechanisms and strategies”, *Chem. Soc. Rev.* **2021**, *50*, 4031.

[11] M. Z. Khan, J. Militky, M. Petru, B. Tomková, A. Ali, E. Tören, S. Perveen, “Recent advances in superhydrophobic surfaces for practical applications: A review”, *European Polymer Journal* **2022**, *178*, 111481.

[12] Y. Tuo, W. Chen, H. Zhang, P. Li, X. Liu, “One-step hydrothermal method to fabricate drag reduction superhydrophobic surface on aluminum foil”, *Applied surface science* **2018**, *446*, 230.

[13] A. M. Alotaibi, S. Sathasivam, B. A. D. Williamson, A. Kafizas, C. Sotelo-Vazquez, A. Taylor, D. O. Scanlon, I. P. Parkin, “Chemical vapor deposition of photocatalytically active pure brookite TiO2 thin films”, *Chem. Mater.* **2018**, *30*, 1353.

[14] M. Ghasemlou, P. H. Le, F. Daver, B. J. Murdoch, E. P. Ivanova, B. Adhikari, “Robust and Eco-Friendly Superhydrophobic Starch Nanohybrid Materials with Engineered Lotus Leaf Mimetic Multiscale Hierarchical Structures”, *ACS Appl. Mater. Interfaces* **2021**, *13*, 36558.

[15] S. Liu, X. Liu, S. S. Latthe, L. Gao, S. An, S. S. Yoon, B. Liu, R. Xing, “Self-cleaning transparent superhydrophobic coatings through simple sol–gel processing of fluoroalkylsilane”, *Applied Surface Science* **2015**, *351*, 897.

[16] T. Darmanin, E. T. De Givenchy, S. Amigoni, F. Guittard, “Superhydrophobic Surfaces by Electrochemical Processes”, *Advanced Materials* **2013**, *25*, 1378.

[17] B. Chen, J. Qiu, E. Sakai, N. Kanazawa, R. Liang, H. Feng, “Robust and Superhydrophobic Surface Modification by a "Paint + Adhesive" Method: Applications in Self-Cleaning after Oil Contamination and Oil-Water Separation”, *ACS Appl. Mater. Interfaces* **2016**, *8*, 17659.

[18] M. Zahid, J. A. Heredia-Guerrero, A. Athanassiou, I. S. Bayer, “Robust water repellent treatment for woven cotton fabrics with eco-friendly polymers”, *Chemical Engineering Journal* **2017**, *319*, 321.

[19] A. Raman, J. S. Jayan, B. D. S. Deeraj, A. Saritha, K. Joseph, “Electrospun Nanofibers as Effective Superhydrophobic Surfaces: A Brief review”, *Surfaces and Interfaces* **2021**, *24*, 101140.

[20] Y. Lin, R. Zhou, J. Xu, “3D printing of superhydrophobic objects with bulk nanostructure”, *Adv Materials Inter* **2018**, *5*, 1801126.

[21] Z. Dong, M. Vuckovac, W. Cui, Q. Zhou, R. H. A. Ras, P. A. Levkin, “3D Printing of superhydrophobic objects with bulk nanostructure”, *Advanced Materials* **2021**, *33*, 2106068.

[22] M. S. Saleh, C. Hu, R. Panat, “Three-dimensional microarchitected materials and devices using nanoparticle assembly by pointwise spatial printing”, Sci. Adv. 2017, 3, e1601986.

[23] D. Zang, S. Tarafdar, Y. Yu. Tarasevich, M. Dutta Choudhury, T. Dutta, “Evaporation of a Droplet: From physics to applications”, *Physics Reports* **2019**, *804*, 1.

[24] S. Nešić, J. Vodnik, “Kinetics of Droplet Evaporation”, *Chemical Engineering Science* **1991**, *46*, 527.

[25] E. B. Secor, “Principles of Aerosol Jet Printing”, *Flexible and Printed Electronics* **2018**, *3*, 035002.

CONTACT

*Ke Zhong, kezhong@andrew.cmu.edu